



Article

Injection Lap Riveting of Aluminum Busbars— A Thermo-Electro-Mechanical Investigation

João P. M. Pragana ¹, Rui F. V. Sampaio ¹, Ivo M. F. Bragança ², Carlos M. A. Silva ¹ and Paulo A. F. Martins ^{1,*}

- ¹ IDMEC, Instituto Superior Técnico, Universidade de Lisboa, Av. Rovisco Pais, 1049-001 Lisboa, Portugal; joao.pragana@tecnico.ulisboa.pt (J.P.M.P.); rui.f.sampaio@tecnico.ulisboa.pt (R.F.V.S.); carlos.alves.silva@tecnico.ulisboa.pt (C.M.A.S.)
- ² CIMOSM, Instituto Superior de Engenharia de Lisboa, Instituto Politécnico de Lisboa, Estr. de Benfica 529, 1549-020 Lisboa, Portugal; ivo.braganca@isel.pt
- * Correspondence: pmartins@tecnico.ulisboa.pt

Abstract: This paper presents a new mechanical joining process to assemble aluminum busbars in energy distribution systems. The process is based on the extension of injection lap riveting to the connection of busbars made from the same material as the rivets and requires redesigning the joints to ensure complete filling with good mechanical interlocking and appropriate contact pressures on the overlapping area. The experimental work was carried out in unit cells and involved the fabrication of the riveted joints and the evaluation of their electrical resistance at different service temperatures. Comparisons with the bolted joints that were fabricated and tested for reference purposes show that injection riveted joints provide lower values of electrical resistance and require much less space for assembly due to the absence of material protrusions above and below their surfaces. Numerical simulation with finite elements allows the relating of the reduction in electrical resistance with the changes in the electric current flow when the bolts are replaced by the new type of rivets. The experimental and numerical predictions revealed that the new type of rivets experience an increase in electrical resistance of up to 6 $\mu\Omega$ (30%) when the service temperature approaches 105 °C. Still, the resistance at this temperature (26.2 $\mu\Omega$) is more than 3 times smaller than that of the bolted joints (80.5 $\mu\Omega$).

Keywords: busbars; mechanical joining; injection lap riveting; electrical resistance; experimentation; finite element method



Citation: Pragana, J.P.M.; Sampaio, R.F.V.; Bragança, I.M.F.; Silva, C.M.A.; Martins, P.A.F. Injection Lap Riveting of Aluminum Busbars—A Thermo-Electro-Mechanical Investigation. *J. Manuf. Mater. Process.* **2022**, *6*, 74. <https://doi.org/10.3390/jmmp6040074>

Academic Editor: Steven Y. Liang

Received: 15 June 2022

Accepted: 4 July 2022

Published: 6 July 2022

Publisher's Note: MDPI stays neutral with regard to jurisdictional claims in published maps and institutional affiliations.



Copyright: © 2022 by the authors. Licensee MDPI, Basel, Switzerland. This article is an open access article distributed under the terms and conditions of the Creative Commons Attribution (CC BY) license (<https://creativecommons.org/licenses/by/4.0/>).

1. Introduction

The importance of electric vehicles in the reduction in greenhouse gas emissions is creating new challenges and opportunities in the design of busbar power distribution systems. On one hand, there is a growing tendency to replace copper busbars with aluminum or copper-aluminum (hybrid) busbars, and on the other hand, there is an increasing demand to improve the overall efficiency of the power distribution systems.

The first trend has been boosted by the appreciation of copper, which rose more than 90% in the last two years [1], but it comes with the price of aluminum having a lower electric conductivity than copper. In practical terms, this means that aluminum busbars require greater cross-sections than copper busbars to ensure the same electric current-carrying capacity. However, this is not a problem for automakers because, as was recently shown by Sampaio et al. [2], aluminum busbars provide 32% mass reduction and 84% cost savings, when compared to copper busbars with similar electric conductance.

The second trend related with the efficiency of the busbar power distribution systems can be approached in several different ways, but the reduction in the electrical resistance of the joints between the busbars is a key aspect of the problem that will be dealt with in this paper.

The joining of busbars can be conducted by means of mechanical- and thermal-based processes (Figure 1) [3]. The mechanical joining processes comprise those in which (i) the forces

are directly applied to the surface of the joints by means of bolts or rivets and those in which (ii) the forces are indirectly applied to the surface of the joints by means of external clamps.

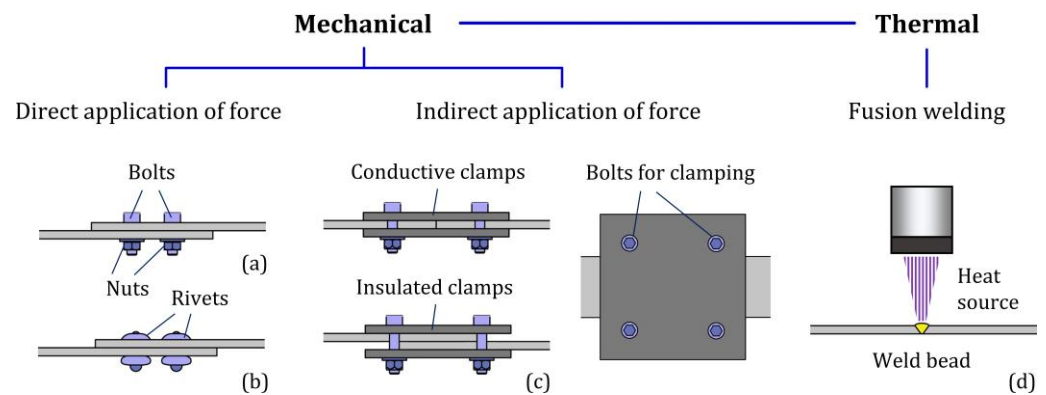


Figure 1. Types of joints used in busbar power distribution systems: (a) bolted joints, (b) riveted joints, (c) clamped joints, and (d) welded joints.

Mechanical joining by means of bolts (Figure 1a) requires the busbars to be partially placed over one another and bolted through the overlapping area. The bolted joints are versatile and easy to assemble and disassemble but have the disadvantage of requiring holes to be drilled or punched through the busbars. The presence of holes in conjunction with the use of bolts gives rise to non-uniform contact pressures through the overlapping areas and causes a distortion of the electric current and an increase in the electrical resistance [4]. A poor surface condition of the busbar overlapping areas and the self-loosening of the bolts are also known to increase the electrical resistance of these joints [5,6].

Mechanical joining by means of conventional rivets [7] (Figure 1b) also requires busbars with pre-drilled or punched holes to be partially placed over one another. Riveting is performed through the overlapping area, and the electric performance of the joints is generally good. However, riveted joints are more difficult to assemble and disassemble than bolted joints, and the head and tail of the rivets, as with the head of the bolts and nuts, give rise to material protrusions above and below their surfaces.

Mechanical joining by application of external clamps may require, or not, partial overlapping of the busbars (Figure 1c). This type of joint is commonly used in busway trunking systems [8], and polymer plates can be used to insulate the clamps from the busbars and minimize the disturbance of the electric current. Clamped joints are easy to assemble and disassemble but are generally more expensive to fabricate and require more space than bolted or riveted joints.

Thermal joining processes generally involve the butt welding of the busbars (Figure 1d) by laser beam welding [9], electron beam welding [10], and plasma arc welding [11]. Despite the current-carrying capacity being practically unaffected by these joints, their use is constrained by the low absorptivity of the busbar materials, the surface preparation requirements, the large busbar thicknesses, and the difficult applicability in situ. Reliability problems also arise in welded joints made from different materials (e.g., aluminum and copper) due to the formation of hard and brittle intermetallic compounds in the weld seam [12].

The search for joining processes capable of increasing the efficiency of the busbar power distribution systems is stimulating the development of new processes that can effectively diminish the electrical resistance of the joints without compromising their reliability and ease of installation. This paper is focused on this goal and presents an innovative, low-cost, and easy-to-use riveting process that minimizes the disturbance of the electric current, while requiring less assembly space than bolted and clamped joints (Figure 2).

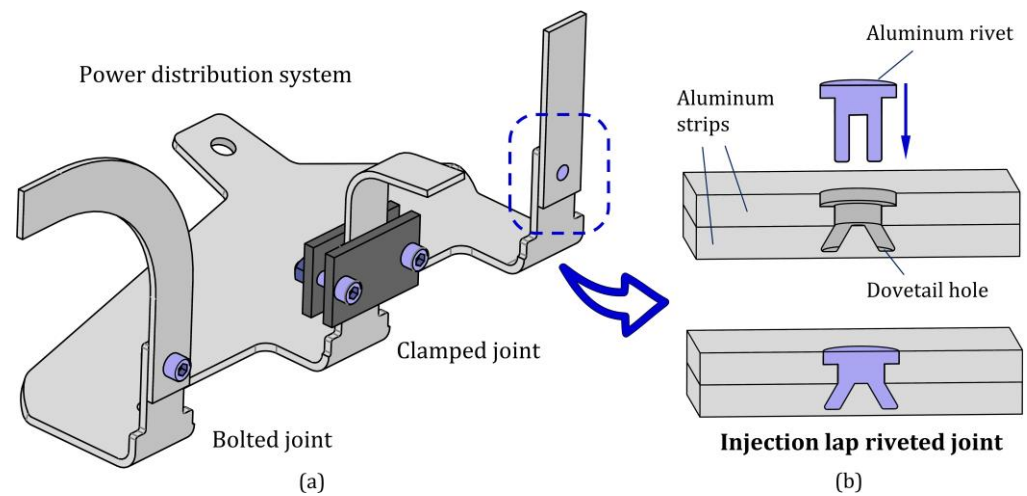


Figure 2. Busbar power distribution system with parallel connections to allow different equipment to operate independently: (a) examples of bolted, clamped, and injection lap riveted joints and (b) detail of the injection lap riveted joint showing the geometry of the rivet and dovetail hole.

The methodology stems from the extension of the applicability domain of injection lap riveting [13], previously developed by the authors for the connection of hybrid busbars made from dissimilar materials (e.g., aluminum and copper), with rivets made from the softer material. The working principle of injection lap riveting is based on plasticity and friction and differs from that of conventional self-pierce riveting, which is based on plasticity, friction, and fracture [13]. Moreover, because the rivets commonly used in self-pierce riveting are made from steel to allow piercing through the busbar strips, the resulting joints will experience larger disturbances of electric current than those which are injection lap riveted.

The challenge to be dealt with in this paper is to redesign the joints to ensure that the injected rivets made from the same material (aluminum) of the busbar strips can provide sound mechanical interlocks and generate adequate contact pressures on the overlapping area.

Finite element modelling, using a thermo-electro-mechanical computer program developed by the authors, gave support to the presentation and allowed the development of a digital twin of the injection lap riveted joint that can replicate the fabrication process and provide estimates of the electrical resistance at different service temperatures.

2. Materials and Methods

The extension of the injection lap riveting process to the connection of aluminum busbars made from the same material as the rivets was built upon an experimental and numerical twofold methodological approach covering (i) the fabrication and (ii) the thermo-electrical characterization of the joints. The work was carried out in unit cells that were representative of the injection lap riveted joints in order to focus attention on the regions of interest (joints) and exclude the remaining geometry of the busbars from the analysis. Comparisons with conventional bolted joints are included for reference purposes.

2.1. Fabrication of the Joints

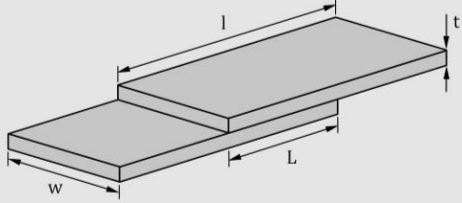
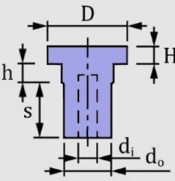
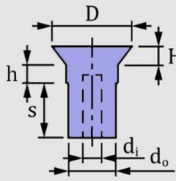
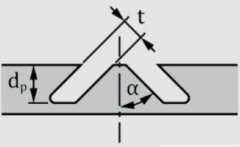
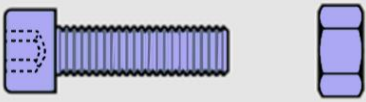
The unit cells of the injection lap riveted joints were made from aluminum AA1050-H111 strips with 100 mm length, 50 mm width, and 5 mm thickness. The overlap L was made equal to the width w , as is common practice in busbars [14], and the ratio L/w between the overlap and the strip thickness was equal to 10 to minimize streamline effects in the electric current [15]. The semi-tubular rivets with an 11.5 mm outer diameter were fabricated from aluminum AA1050-O rods with a 20 mm diameter.

The unit cells of the bolted joints were made from the same aluminum AA1050-H111 strips and M8 medium carbon steel (class 8.8) hexagonal socket head bolts and nuts.

The injection lap riveted joints were fabricated at ambient temperature by forcing the semi-tubular rivets into the pre-drilled holes of the overlapped strips. These consisted of counterbore or countersunk holes in the strips that were placed on the punch side, and dovetail ring holes in the strips that were placed on the opposite side. Different hole and rivet geometries were analyzed to ensure good mechanical interlockings with low electrical resistances.

The bolted joints required through holes of 8.4 mm diameter to be pre-drilled in both strips and fastened by application of a 20 Nm tightening torque on the M8 hexagonal socket head bolts. The aluminum strips were utilized without surface preparation in both types of unit cells, and further details on their geometries and process parameters are given in Table 1.

Table 1. Geometry and process parameters of the unit cells corresponding to the injection lap riveted and bolted joints.

Strips									
	AA1050-H111 aluminum	$l \times w \times t: 100 \times 50 \times 5 \text{ (mm}^3\text{)}$							
Surface preparation	As supplied								
Injection lap riveted joints									
	Counterbored rivet	Countersunk rivet							
Process parameters	d_i (mm)	d_o (mm)	D (mm)	H (mm)	h (mm)	s (mm)	α (°)	d_p (mm)	t (mm)
	2.1 ± 0.1	6.6 ± 0.1	11.3, 11.8	2	3	4.3–7.9	15, 30	3, 4	2.3 ± 0.1
Bolted joints									
	Process parameters	Material	Size	Tightening torque (Nm)					
	Medium carbon steel (class 8.8)	M8	20						

Finite element modelling of the injection lap riveting and tightening torque processes required mechanical characterization of the AA1050-H111 strips, AA1050-O rivets, and medium carbon steel bolts at ambient temperature. This was carried out by means of tensile and compression tests, in which tensile specimens were extracted from the AA1050-H111 strips and tested in accordance with the ASTM standards E8/E8 M [16], and compression specimens with a 20 mm height and 20 mm diameter were extracted from the AA1050-O rods that were used to fabricate the semi-tubular rivets. The tests were performed in an Instron 4507 universal testing machine, and Table 2 provides a summary of the mechanical properties of the materials. The data for the medium carbon steel of the bolts were taken from the literature [17,18].

Table 2. Mechanical properties of the materials.

	AA1050-H111	AA1050-O	Steel (Class 8.8)
Elastic modulus (GPa)	69	69	205
Poisson ratio	0.33	0.33	0.29
Yield strength (MPa)	34	28	640
Ultimate tensile strength (MPa)	83	76	800
Stress-strain curve (MPa)	$\sigma = 109 \epsilon^{0.17}$	$\sigma = 140 \epsilon^{0.24}$	-

2.2. Thermo-Electrical Characterization of the Materials and Joints

The experimental apparatus shown in Figure 3 was utilized to perform the thermo-electrical characterization of the aluminum AA1050 and of the unit cells corresponding to the injection lap riveted and bolted joints. The specimens were fixed along their edges in two copper blocks and connected to an AC transformer (OFICEL 1.5 kVA). The temperature was measured by thermal imaging and required painting the strips, rivets, and bolts in black to ensure equal values of emissivity. The thermal imaging equipment utilized in the experiments consisted of an

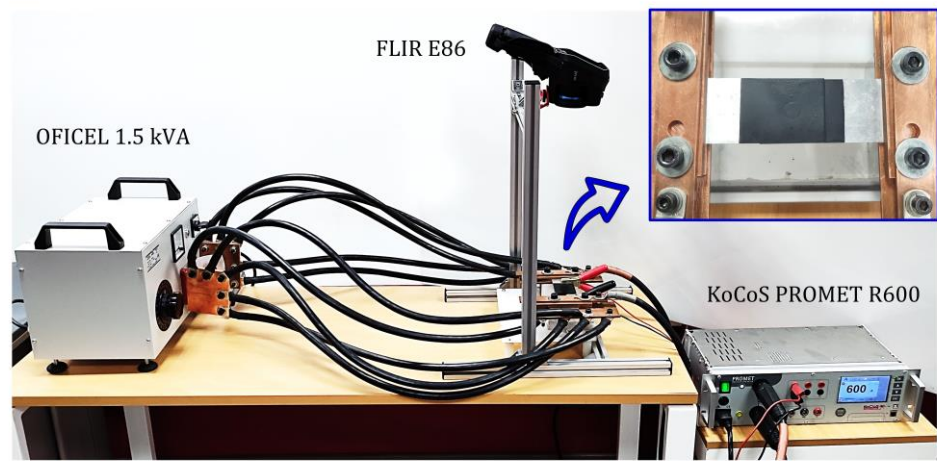
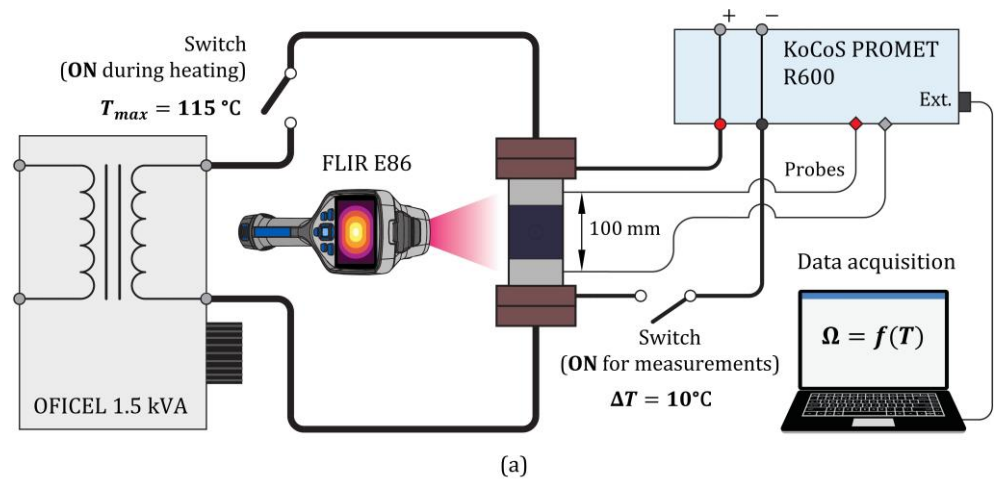


Figure 3. (a) Layout and (b) photograph of the experimental apparatus that was utilized to perform the thermo-electrical characterization of the materials and joints.

The experimental procedure consisted in supplying an electric current of 1500 A for approximately 10 to 20 min to raise the temperature of the specimens by Joule effect up to a maximum value $T_{max} = 115 \text{ °C}$ (at the center). The temperature was measured by thermal imaging and required painting the strips, rivets, and bolts in black to ensure equal values of emissivity. The thermal imaging equipment utilized in the experiments consisted of an

infrared camera (FLIR E86) equipped with a focal plane array microbolometer detector, 464×348 resolution, and a spectral range of 7.5 to 14 μm .

Once the maximum temperature $T_{max} = 115 \text{ }^\circ\text{C}$ was reached, the transformer was switched off, and the specimens began to cool down by convection and radiation to the environment. The electric resistance of the unit cells was determined in the cooling stage, starting at $T_0 = 105 \text{ }^\circ\text{C}$, to cope with the limiting temperature defined by the IEEE standard for metal-clad switchgears [19], and finishing at the ambient temperature of $20 \text{ }^\circ\text{C}$.

The electric resistance was determined by means of a four-point probe technique [20], and the two measuring probes were spaced 100 mm apart and connected to a micro-ohmmeter KoCoS PROMET R600 supplying an electric current of 600 A for approximately 2 s. The voltage drop V measured by the probes allowed the determining of the electric resistance by means of the Ohm's law. The procedure was repeated each time the drop in temperature between two successive measurements was equal to $\Delta T = T_{n+1} - T_n = 5 \text{ }^\circ\text{C}$.

Thermo-electrical finite element modelling of the unit cells required knowledge of the evolution of the electric resistivity with temperature. The evolution for the aluminum AA1050 was determined from the electrical resistance measurements that were performed in the above-mentioned experimental apparatus. The results are given in Figure 4 and consist of straight lines rising from left to right as the temperature increases. The electric resistivity of the medium carbon steel was retrieved from the literature [21] and presents values that are approximately three times higher than those of aluminum AA1050. The steel values also have larger variations of electric resistivity with temperature.

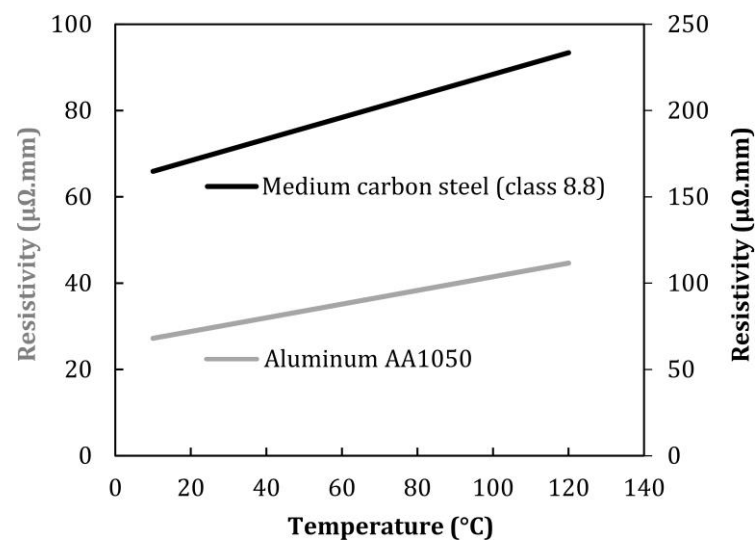


Figure 4. Electric resistivity of aluminum AA1050 (left vertical axis) and medium carbon steel (class 8.8) (right vertical axis) as a function of temperature.

2.3. Numerical Modelling

Numerical modelling followed the experimental twofold methodological approach. On one hand, there was a need to simulate the mechanical joining stage corresponding to the fabrication of the injection lap riveted and bolted unit cells, and on the other hand, it was necessary to simulate the thermo-electrical stage corresponding to the flow of electric current for measuring the electrical resistance of the unit cells at different service temperatures.

Both types of simulations were carried out in the finite element computer program i-form, developed by the authors [22], which is built upon an extension of the flow formulation to include elastic effects and couples the quasi-static governing equilibrium equations with the electric potential and the heat transfer equations.

The weak forms of the governing mechanical (1), electrical (2), and thermal (3) equations for a continuous body with a control volume V , bounded by a closed surface S

consisting of a region S_t where tractions t_i are applied and a region S_q where the heat flux q_n containing the heat dissipated by convection and radiation is defined, are given by,

$$\int_V \sigma'_{ij} \delta D_{ij} dV + \int_V K D_v \delta D_v dV - \int_{S_t} t_i \delta u_i dS = 0 \tag{1}$$

$$\int_V \nabla^2 \Phi \delta \Phi dV = 0 \tag{2}$$

$$\int_V k \nabla T \nabla (\delta T) dV - \int_{S_q} q_n \delta T dS_q + \int_V \rho c \frac{dT}{dt} \delta T dV - \int_V \beta \sigma_{ij} D_{ij} \delta T dV = 0 \tag{3}$$

In the above equations, the velocity u_i , the electric potential Φ , and the temperature T are the primary unknowns. The remaining symbols are the deviatoric Cauchy stress σ'_{ij} , the rate of deformation D_{ij} , the volumetric rate of deformation D_v with the associated penalty function K , the thermal conductivity k , the specific heat capacity ρc , and the fraction β of plastic work converted into heat.

Mechanical joining by injection lap riveting was simulated under rotational symmetric conditions because forcing the semi-tubular rivets into the dovetail ring holes of the strips placed on the opposite punch side gives rise to axisymmetric plastic deformation in the rivets and neighborhood strip materials. Figure 5a shows the finite element mesh at the beginning and the end of the injection lap riveting process, in which the cross-section of the rivets and strips was discretized by means of approximately 5000 quadrilateral elements. The flat compression punch and die were considered as rigid objects and discretized by means of linear friction elements. The CPU time for modelling the mechanical joining by injection lap riveting was roughly 90 min in a computer equipped with an Intel Core i7-6950X processor.

The thermo-electric simulations for determining the evolution of the electric current density and the electrical resistance with temperature required the utilization of three-dimensional models with a half-width size of the unit cells utilized in the experiments. A thin interface layer with 0.05 mm thickness was included to simulate the influence of the surface roughness and the oxide films along the overlapping area between the aluminum strips. The discretization of the strips and interface layer was performed with approximately 50,000 hexahedral elements. The copper blocks were modelled as rigid objects and their contours underwent discretization by means of spatial triangular elements.

The modelling strategy followed the experimental procedure that was previously described to perform the thermo-electrical characterization of the joints. The first part consisted of a thermal simulation of the unit cells subjected to Joule heating due to an electric current of 1500 A supplied by the transformer for approximately 10 min.

The second part started after achieving the target temperature $T_{max} = 115 \text{ }^\circ\text{C}$ at the center of the unit cells and consisted of modelling the cooling by convection and radiation to the environment after switching off the transformer. The electrical resistance measurement instants, during which the micro-ohmmeter supplied an electric current of 600 A for approximately 2 s, were modelled by coupling the thermal and electric modules of the finite element computer program in a staggered manner.

The simulation of the bolted unit cells made exclusive use of three-dimensional models, in which the mechanical simulations were used to replicate the tightening torque of 20 Nm, and the thermal and electrical simulations were used to replicate the heating, cooling, and electrical resistance measurement stages. The results of these simulations will be presented in the following sections of the paper.

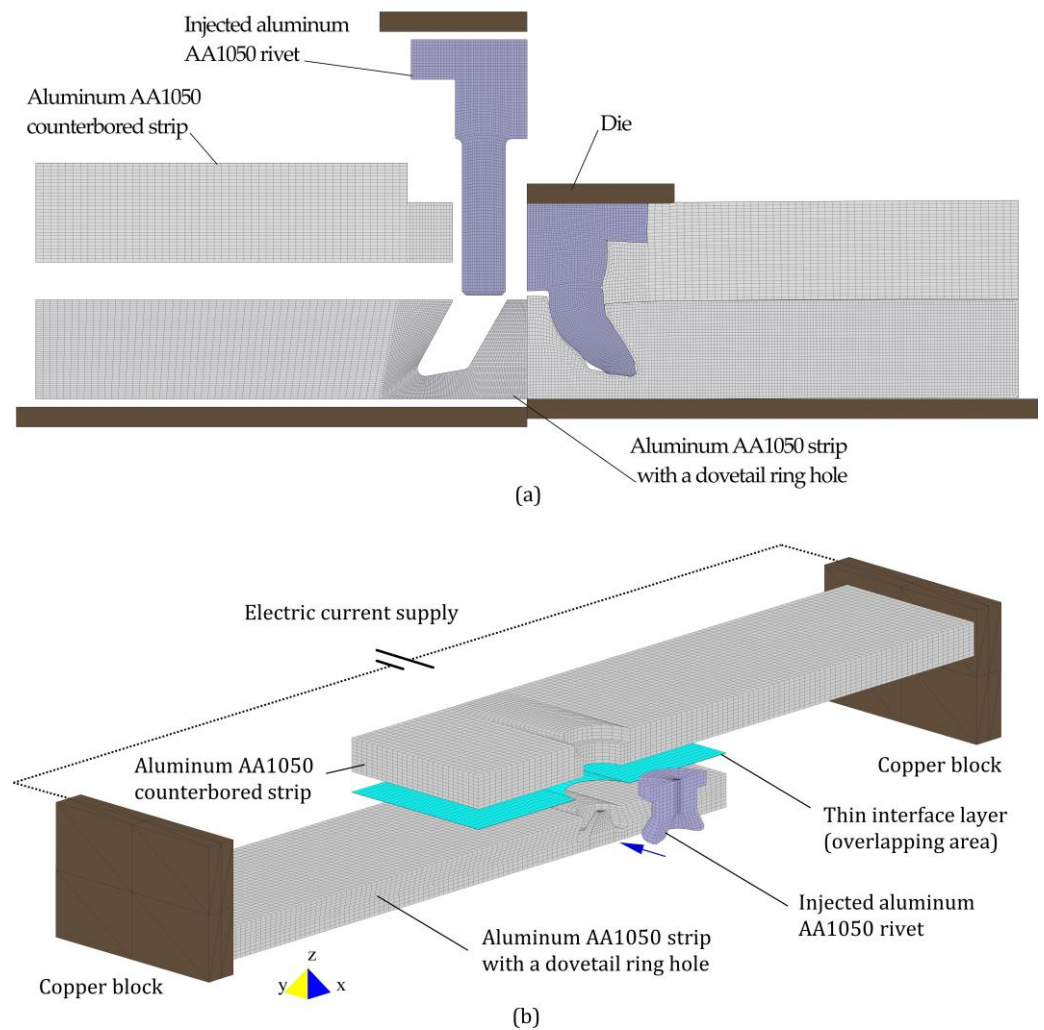


Figure 5. Finite element modelling of the injection lap riveted unit cells showing (a) a rotational symmetric model utilized in the simulation of mechanical joining at the beginning and at the end of the process and (b) a three-dimensional model utilized in the thermo-electric simulation.

3. Results and Discussion

3.1. Injection Lap Riveting

The finite element simulation of injection lap riveting focused on the combined influence of the different process parameters included in Table 1, namely (i) the inclination angle α and (ii) the depth d_p of the dovetail ring holes and (iii) the geometry (countersunk or counterbored) of the rivet heads. Concerning the inclination angle α of the dovetail ring holes, it may be concluded from Figure 6 that the countersunk rivet head geometries with small inclination angles (say, $\alpha = 15^\circ$) give rise to small interlockings, incomplete filling of the dovetail ring holes, and low contact pressures (below 100 MPa) between the strips and between the strips and rivets (refer to the radial stress in Figure 6a), through which most of the electric current flows.

Raising the inclination angle α to 30° helps to improve the quality of the injection lap riveted joints because the interlocking becomes larger, and the contact pressures can reach values of up to 200 MPa (Figure 6b). However, filling of the dovetail ring hole remains incomplete, which will negatively affect the overall electric performance of the joints.

Similar results are obtained from the analysis of the vertical contact pressure between the strips in both cases ($\alpha = 15^\circ$ and $\alpha = 30^\circ$). This conclusion is very important because the electric contact resistance R of the joints is dependent on the square root of the contact

pressure [23], due to its role in breaking the oxide films and flattening the asperities by plastic deformation.

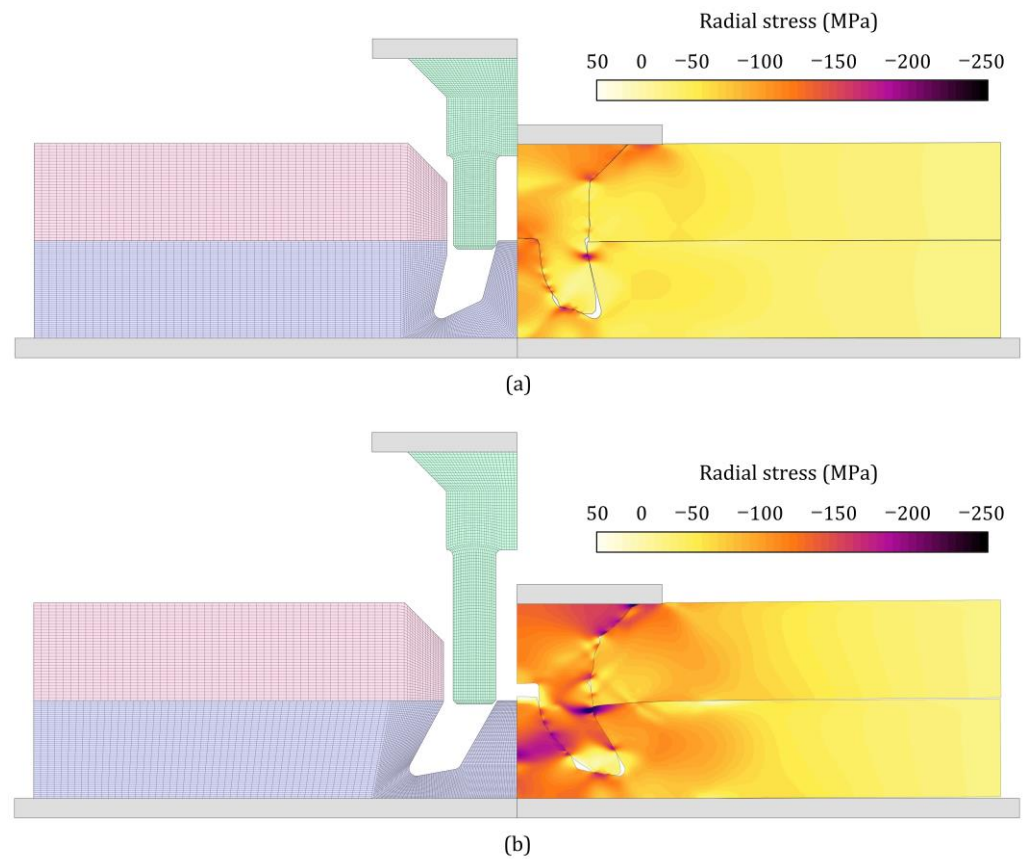


Figure 6. Finite element simulation of injection lap riveting with countersunk head rivets showing the mesh at the beginning (left) and the distribution of radial contact pressure (MPa) at the end of the stroke (right) for two-unit cells corresponding to (a) $\alpha = 15^\circ$, $d_p = 4$ mm and (b) $\alpha = 30^\circ$, $d_p = 4$ mm.

The attempt to use shallower dovetail holes ($d_p = 3$ mm) to ensure complete filling of the cavities exacerbates the problem, as shown in Figure 7. In fact, not only do the unfilled pockets represent a greater percentage of the total cavity volume, but also the interlocking and contact pressures become substantially smaller than in the case of the deeper dovetail holes with $d_p = 4$ mm (Figure 6b).

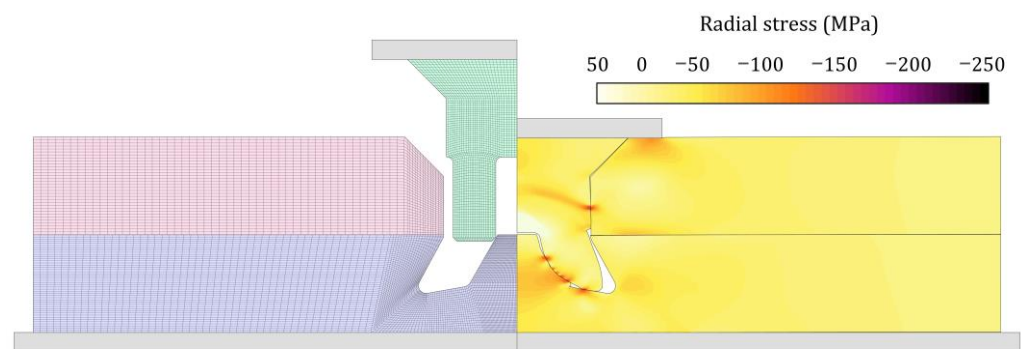


Figure 7. Finite element simulation of injection lap riveting countersunk head rivets, showing the mesh at the beginning (left) and the distribution of radial contact pressure (MPa) at the end of the stroke (right) for unit cells with $\alpha = 30^\circ$, $d_p = 3$ mm.

The difficulties that were encountered in filling the dovetail holes with the countersunk head rivets are mainly caused by the plastic deformation of the holes as the rivet is injected by compression. This problem results from the fact that the rivets and strips are made from aluminum AA1050 with similar mechanical strength and had never been observed with this importance by the authors [13]. The reason is because previous work was carried out with dissimilar materials, in which the dovetail holes were pre-drilled in the stronger strips and the rivets were made from the material of the softer strips.

The solution by which to minimize the unfilled pockets inside the dovetail ring holes and, at the same time, to ensure a good mechanical interlocking and contact pressure between the strips and the rivet involved modifying the rivet head by introducing a counterbored geometry (Figure 8).

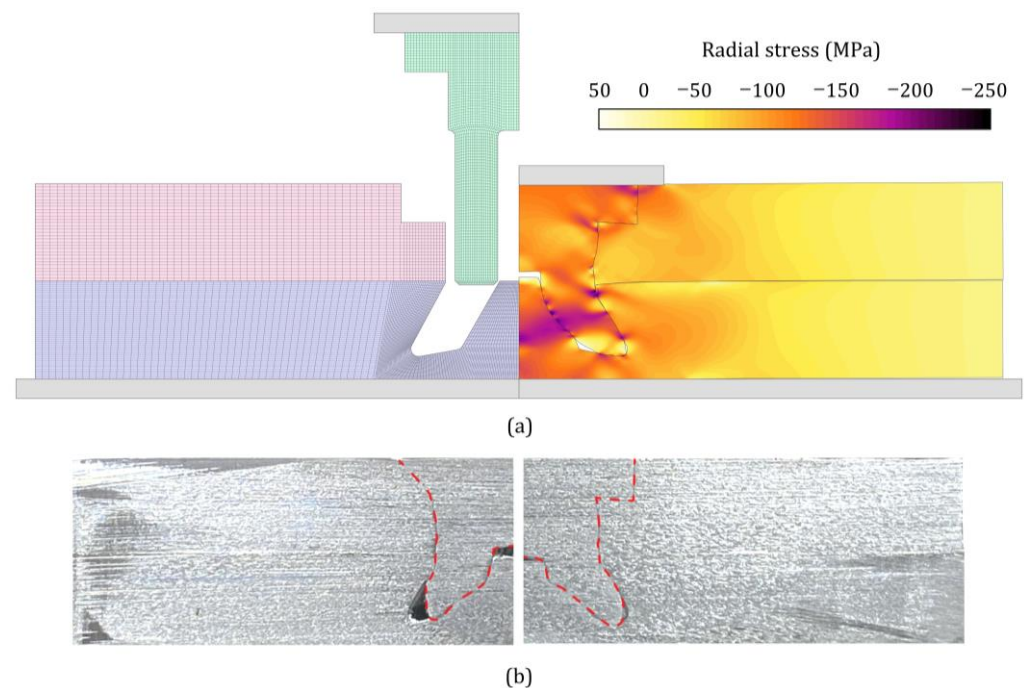


Figure 8. Finite element simulation of injection lap riveting counterbored head rivets showing (a) the mesh at the beginning (left) and the distribution of radial contact pressure (MPa) at the end of stroke (right) for unit cells with $\alpha = 30^\circ$, $d_p = 4$ mm and (b) a photograph of a cross-section where the counterbored head rivet (right) is compared with that obtained using a countersunk geometry (left).

As seen, the counterbored head rivets can provide contact pressures above 200 MPa, without causing bending of the strips and large plastic deformation of the dovetail ring holes during injection by compression. The filling of the dovetail ring hole is also good, as can be inferred from the photograph of the cross-section taken from an experimental unit cell (Figure 8b-right) and from the mesh details that are included in the riveting force vs. the punch stroke evolution of Figure 9.

The comparison with the cross-section geometry of a unit cell fabricated with a countersunk rivet (Figure 8b-left) head also confirms the advantage of the counterbored geometry (Figure 8b-right) in providing a better filling of the dovetail ring hole.

Regarding the finite element and experimental evolutions of the riveting force with the compression punch stroke, three main stages may be distinguished. The initial stage (labelled as 'A' in Figure 9) is associated with the sliding with friction of the rivet inner wall along the inward dovetail hole surface. The second stage, labelled as 'B', corresponds to a region of the graphic in which the force grows moderately with the punch stroke up to an instant of time corresponding to the contact between the rivet end and the dovetail hole end.

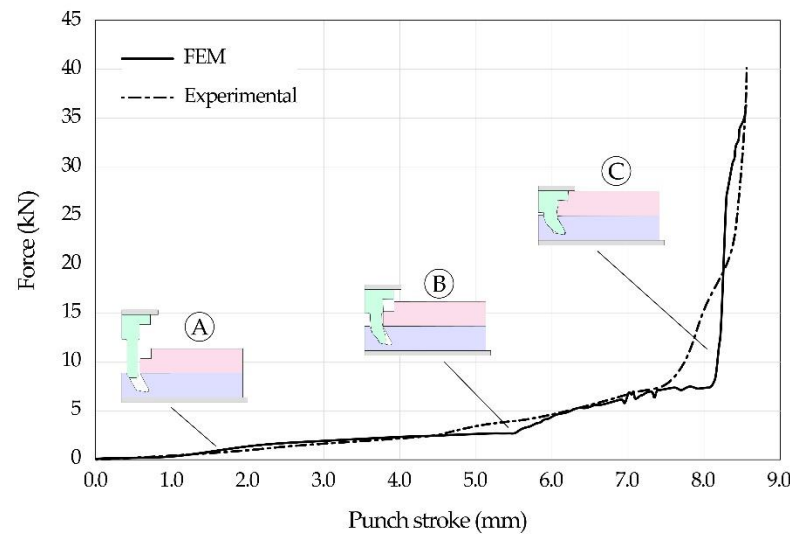


Figure 9. Experimental and finite element predicted evolution of the riveting force with punch stroke for a counterbored head rivet with $\alpha = 30^\circ$, $d_p = 4$ mm. The mesh details are taken from each of the three deformation stages.

The final stage labelled as ‘C’ is characterized by a sharp increase in the force due to the compression of the counterbored rivet head against the strip.

3.2. Thermo-Electro Characterization of the Joints

Figure 10 provides a comparison between the experimental and the finite element predicted distributions of temperature for an instant of time corresponding to a temperature of 85°C at the center of the injection lap riveted and bolted joints. As seen in Figure 10a, the agreement between the experimental and numerical results obtained for the injection lap riveted joint is good, showing a relatively uniform distribution of temperature, with small differences between the highest values of the center (85°C) and the lowest values (75°C) next to the copper blocks where the unit cell was fixed and connected to the micro-ohmmeter supplying an electric current of 600 A for approximately 2 s.

The results obtained for the bolted joint (Figure 10b) are different because they show a larger concentration of temperature in the bolt, with values approximately 30°C higher than those found next to the copper blocks. Because the disturbance in temperature distribution due to Joule heating is a direct consequence of the disturbance in the electric current, one may conclude that injection lap riveted joints provide smaller electrical resistance values than bolted joints. This is confirmed in Figure 11, which shows the average electrical resistance values of the injection lap riveted (IJL) joints to be 3.2 times smaller than those of the bolted (B) joints.

The experimental procedure for determining the electrical resistance of the injection lap riveted joints at different temperatures was previously described in Section 2.3, and the results shown in Figure 11 allow the conclusion that the experimental and numerical electrical resistances vary linearly over the entire temperature range. The variations correspond to an increase of approximately $6\ \mu\Omega$ in the case of the injected lap riveted joints and $18\ \mu\Omega$ in the case of the bolted joints.

The black dashed line in Figure 11 corresponds to the finite element predictions for an ideal joint made from two aluminum strips in perfect contact, without auxiliary joining elements and no contaminant and oxide films along their overlapping area. Comparison against the results obtained for the injection lap riveted and bolted unit cells allows the conclusion that bolted joints provide electrical resistance values 7 times higher than an ideal joint, whereas injection lap riveted joints provide electrical resistance values only 2.2 times higher.

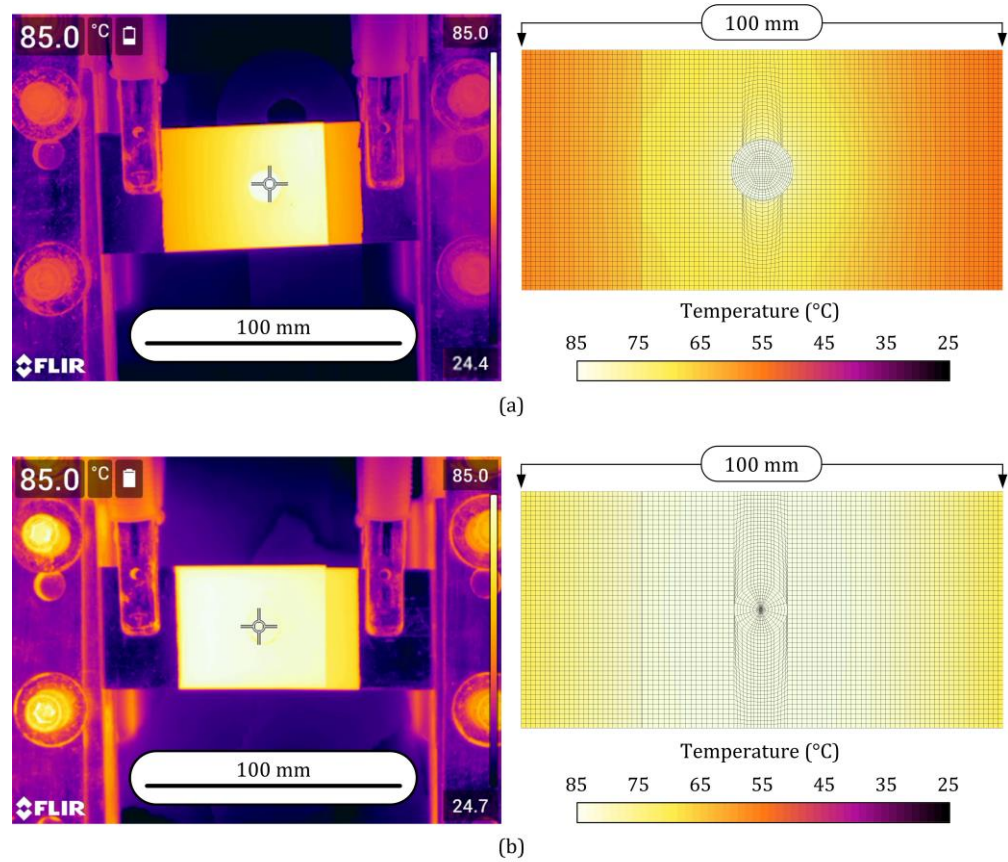


Figure 10. Experimental and finite element predicted distribution of temperature for an instant corresponding to a temperature of 85 °C at the center of the (a) injection lap riveted and (b) bolted joints.

The reason for the discrepancies in the results obtained with the two different types of unit cells results from the fact that electric current mainly flows through the bolts and rivets due to the inability of the AA1050 aluminum strips to generate enough contact pressures along the overlapping area to break the hard Al_2O_3 oxides. This is confirmed by the finite element predictions of current density j shown in Figure 12a,b.

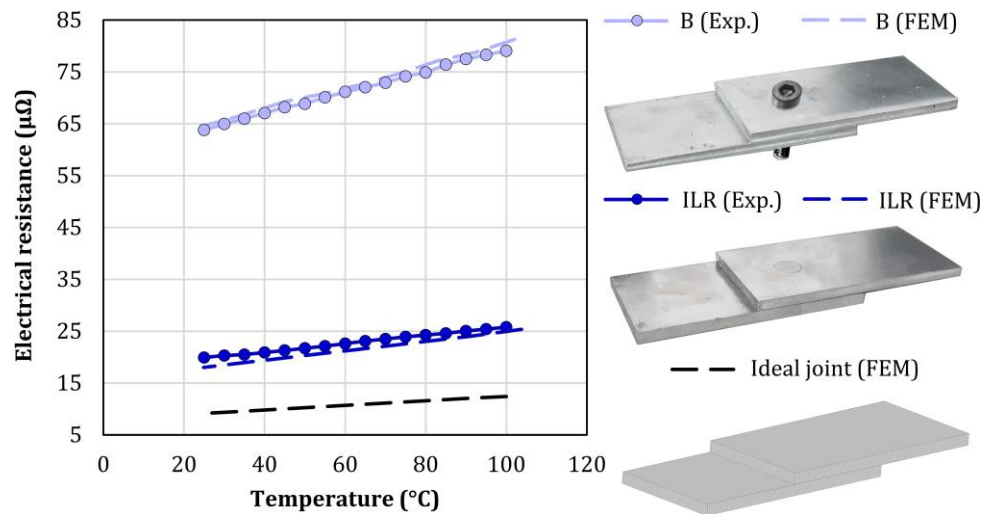


Figure 11. Experimental and finite element predicted evolutions of the electrical resistance with temperature.

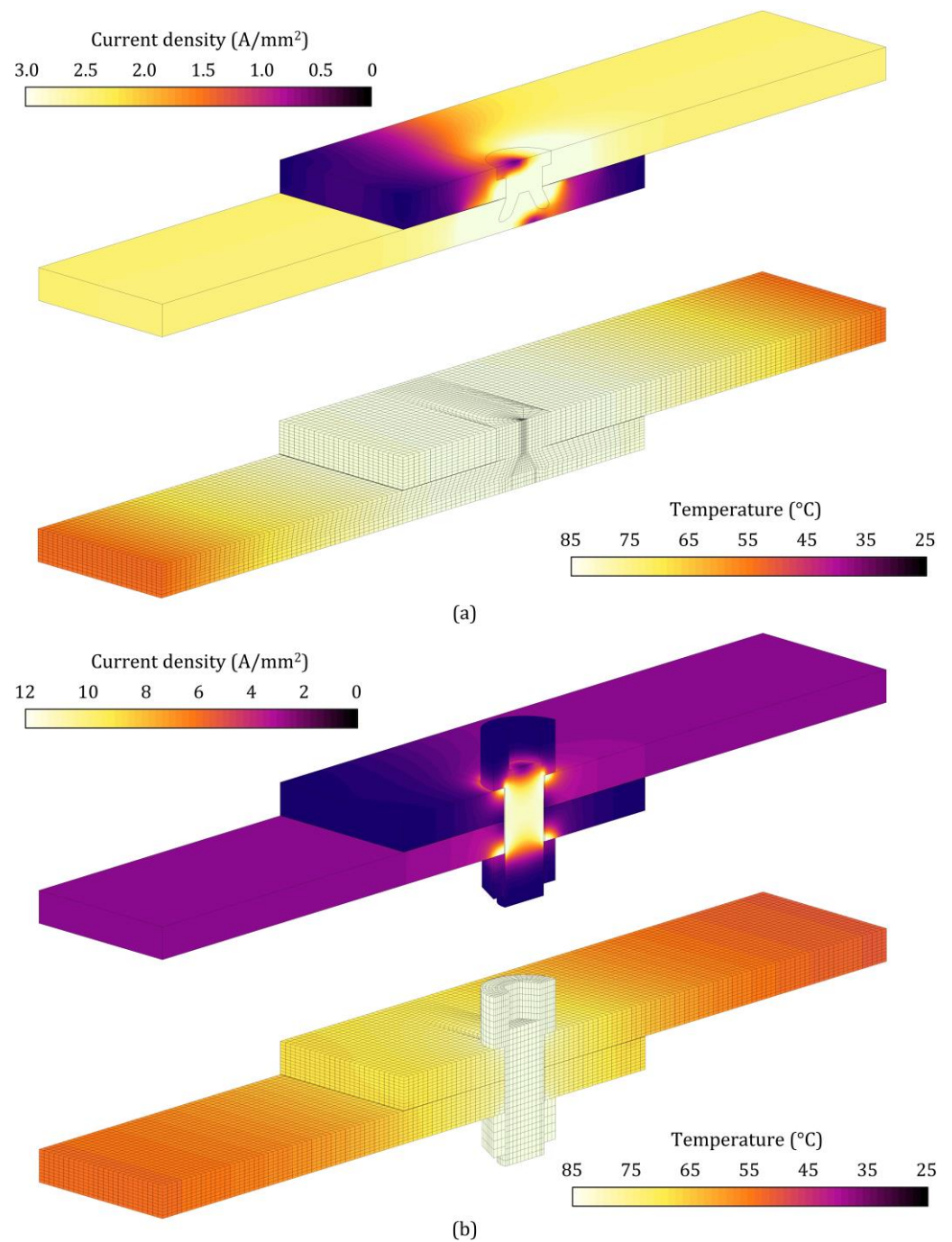


Figure 12. Finite element predicted distributions of electric current density (A/mm²) and temperature (°C) for the (a) injection lap riveted (counterbored) and (b) bolted unit cells when the temperature at the center is equal to 85 °C (during the cooling stage).

In fact, the highest current density j values of approximately 12 A/mm² that are found in the bolt (Figure 12b) are in close agreement with the electric current of 600 A, supplied by micro-ohmmeter during the measuring stage, flowing almost exclusively through the cross section of the M8 hexagonal socket head bolt,

$$j = \frac{600}{\pi \cdot 4^2} = 11.9 \text{ A/mm}^2 \quad (4)$$

The finite element predictions of electric current density near the copper fixing blocks (Figure 12a,b) also cope with the expected analytical values resulting from the 600 A supplied by the micro-ohmmeter flowing through the 50 mm × 5 mm cross-section of the aluminum strips,

$$j = \frac{600}{50 \cdot 5} = 2.4 \text{ A/mm}^2 \tag{5}$$

The finite element predicted distribution of temperature included in Figures 12a and 13b helps in further corroborating the previously mentioned results because the electric current, in the case of the bolted joints, is mainly flowing from one strip to the other through the small cross-section of the steel bolts with an electric resistivity 6 times higher than that of aluminum (refer to Figure 4).

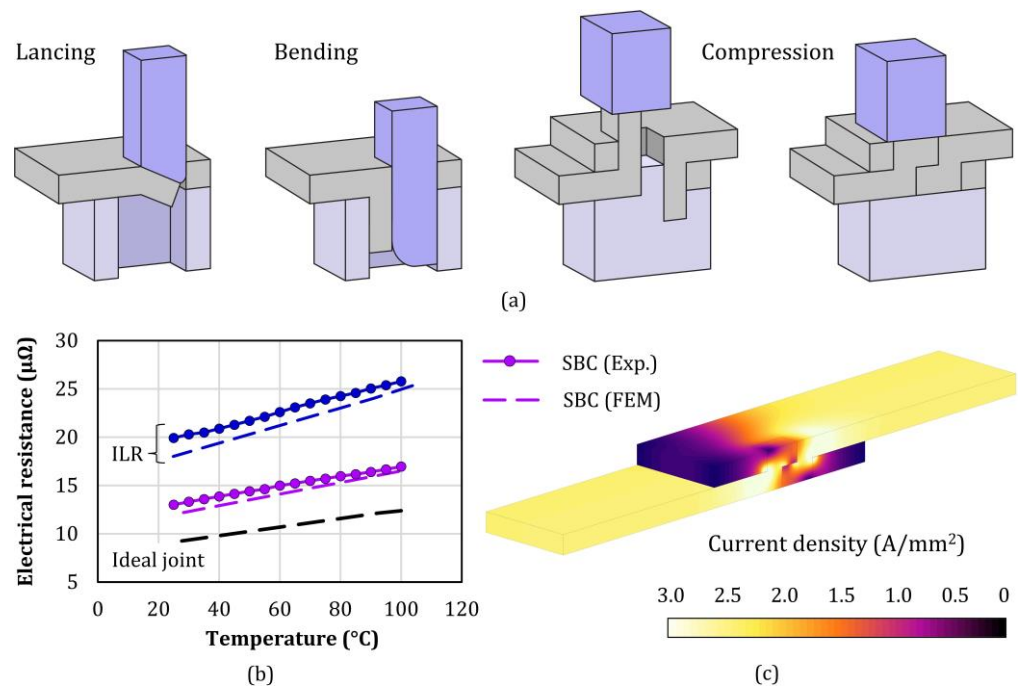


Figure 13. Sheet-bulk compression (SBC) of aluminum busbar joints: (a) schematic view of the fabrication process, (b) experimental and finite element predicted evolutions of the electrical resistance with temperature, and (c) finite element predicted distributions of electric current density (A/mm²) when the temperature at the center is equal to 85 °C.

3.3. Future Research Directions

Injection lap riveting with counterbored semi-tubular rivets offers significant gains in the electrical resistance of aluminum busbar joints when compared to countersunk head riveted and bolted joints. However, the overall electrical resistance values are still 2 times higher than those of an ideal joint without auxiliary elements and oxide films along the overlapping area.

Future research directions should therefore privilege the development of joining processes without auxiliary elements that can generate high contact pressures along the overlapping area. In the case of aluminum busbars produced in large batches, a possible future direction is to make use of joining by sheet-bulk compression, which was previously developed by the authors to assemble the strip or sheet conductors in progressive tool systems comprising a sequence of lancing, bending, and compression operations [24] (Figure 13a).

Experimental and finite element simulation work performed in joining by sheet-bulk compression (SBC) of aluminum AA1050 unit cells unveils electrical resistances varying from 12.7 μΩ to 17.2 μΩ, when the temperature increases from 20 °C to 105 °C (Figure 13b).

This means shortening by nearly half the distance to the values provided by the ideal busbar joint due to smaller variations in the electric current density (Figure 13c) than those obtained in the injection lap riveted joints (Figure 12a).

The conclusion is that for applications in situ, in which sheet-bulk compression cannot be employed, there is still room to further develop the injection lap riveting (ILR) process to obtain better electric performances. The drawback resulting from the necessity of pre-drilling the dovetail ring holes cannot be seen as an exclusive limitation of injection lap riveting because conventional bolted joints also require pre-drilling (or punching) through holes in the busbar strips. In fact, the main limitation of the process, which required the redesigning of the joints, has to do with plastic deformation and friction along the contact interfaces between the rivets and the dovetail ring holes in strips made from the same material as the rivets.

4. Conclusions

The extension of the injection lap riveting process to the in-situ connection of busbars made from the same material as the rivets is feasible and capable of ensuring good electric performances. The main conclusions drawn from the experimental and numerical work performed in aluminum AA1050 unit cells are the following:

- Injection lap riveted joints require much less space for assembly than alternative solutions based on conventional bolting or riveting due to the absence of material protrusions above and below the joint surfaces.
- Semi-tubular rivet heads must have counterbored geometries and appropriate shank lengths to ensure complete filling with good mechanical interlocking and appropriate contact pressures on the overlapping areas between the two busbar strip conductors.
- Injection lap riveted joints built upon semi-tubular counterbored head rivets provide electrical resistances more than 3 times smaller than those of bolted joints due to the replacement of the steel bolts by aluminum rivets, causing smaller electric current disturbances.
- The sensitivity of the electrical resistance to temperature variations is also smaller for the injection lap riveted joints, which experience an increase of just $6 \mu\Omega$ when the temperature is raised from 20°C to 105°C .
- Future developments must account for the differences between the in situ and the factory assembly of busbar systems because in the case of the latter, the new solution based on joining by sheet-bulk compression can provide electrical resistances 35% smaller than those obtained by the newly proposed injection lap riveting process.

Author Contributions: Conceptualization, I.M.F.B., C.M.A.S. and P.A.F.M.; methodology, I.M.F.B., C.M.A.S. and P.A.F.M.; software, R.F.V.S., J.P.M.P. and P.A.F.M.; validation, R.F.V.S. and J.P.M.P.; formal analysis, R.F.V.S., J.P.M.P., I.M.F.B., C.M.A.S. and P.A.F.M.; investigation, R.F.V.S., J.P.M.P., I.M.F.B., C.M.A.S. and P.A.F.M.; resources, I.M.F.B., C.M.A.S. and P.A.F.M.; writing—original draft preparation, P.A.F.M.; writing—review and editing, R.F.V.S., J.P.M.P., I.M.F.B., C.M.A.S. and P.A.F.M.; visualization, R.F.V.S. and J.P.M.P.; supervision, I.M.F.B., C.M.A.S. and P.A.F.M.; project administration, P.A.F.M.; funding acquisition, P.A.F.M. All authors have read and agreed to the published version of the manuscript.

Funding: This research was funded by Fundação para a Ciência e a Tecnologia of Portugal and IDMEC under LAETA-UIDB/50022/2020 and PTDC/EME-EME/0949/2020.

Institutional Review Board Statement: Not applicable.

Informed Consent Statement: Not applicable.

Data Availability Statement: All data supporting the reported results are available in the paper.

Acknowledgments: The authors would like to thank the support provided by Fundação para a Ciência e a Tecnologia of Portugal and IDMEC under LAETA-UIDB/50022/2020 and PTDC/EME-EME/0949/2020.

Conflicts of Interest: The authors declare no conflict of interest.

References

1. YCharts. Available online: http://ycharts.com/indicators/copper_price (accessed on 26 May 2022).
2. Sampaio, R.F.; Zwicker, M.F.; Pragana, J.P.; Bragança, I.M.; Silva, C.; Nielsen, C.V.; Martins, P.A. Busbars for e-mobility: State-of-the-art review and a new joining by forming technology. In *Mechanical and Industrial Engineering: Historical Aspects and Future Directions*; Davim, J.P., Ed.; Springer: Berlin, Germany, 2022; pp. 111–141.
3. Bao, Y.J.; Cheng, K.W.E.; Ding, K.; Wang, D.H. The study on the busbar system and its fault analysis. In Proceedings of the 5th International Conference on Power Electronics Systems and Applications (PESA), Hong Kong, China, 11–13 December 2013; pp. 1–7.
4. Tzeneva, R.; Slavtchev, Y.; Mladenov, V. New connection design of high-power bolted busbar connections. In Proceedings of the 11th WSEAS International Conference on Circuits, Agios Nikolaos, Greece, 23–25 July 2007; pp. 228–233.
5. Sampaio, R.F.V.; Pragana, J.P.M.; Bragança, I.M.F.; Silva, C.M.A.; Nielsen, C.V.; Martins, P.A.F. Electric performance of fastened hybrid busbars: An experimental and numerical study. *J. Mater. Des. Appl.* **2021**, *236*, 1152–1163. [[CrossRef](#)]
6. Moustafa, G.; Grossmann, S.; Abdel-Salam, M.; Dessouky, S.S.; El-Makkawy, S.M. Joint resistance of bolted copper bus-bar connections as influenced by mechanical contact devices material and configuration. In Proceedings of the 13th Middle East Power Systems Conference (MEPCON), Assiut, Egypt, 20–23 December 2009; pp. 300–305.
7. Chapman, D.; Norris, T. *Copper for Busbars: Guidance for Design and Installation*; Copper Development Association: New York, NY, USA, 2014; pp. 90–102.
8. Rana, B.; Mallick, P.; Rana, T.K.; Basu, D.; Biswas, A.N.; Pramanik, S. Efficient and superior elbow joint for high power busway trunking system. In Proceedings of the 8th Annual Industrial Automation and Electromechanical Engineering Conference (IEMECON), Bangkok, Thailand, 16–18 August 2017; pp. 16–21.
9. Katayama, S. Introduction: Fundamentals of laser welding. In *Handbook of Laser Welding Technologies*; Katayama, S., Ed.; Woodhead Publishing: Cambridge, UK, 2013; pp. 3–16.
10. Moschinger, M.; Mittermayr, F.; Enzinger, N. Influence of beam figure on porosity of electron beam welded thin-walled aluminum plates. *Materials* **2022**, *15*, 3519. [[CrossRef](#)] [[PubMed](#)]
11. Xu, B.; Tashiro, S.; Jiang, F.; Chen, S.; Manabu, T. Effect of arc pressure on the digging process in variable polarity plasma arc welding of A5052P aluminum alloy. *Materials* **2019**, *12*, 1071. [[CrossRef](#)] [[PubMed](#)]
12. Schmidt, P.A.; Schweier, M.; Zaeh, M.F. Joining of lithium-ion batteries using laser beam welding: Electrical losses of welded aluminum and copper joints. In Proceedings of the ICALEO—International Congress on Applications of Lasers & Electro-Optics, Temecula, CA, USA, 23–27 September 2012; pp. 915–923.
13. Ferreira, F.R.; Pragana, J.P.M.; Bragança, I.M.F.; Silva, C.M.A.; Nielsen, C.V.; Martins, P.A.F. Injection lap riveting. *CIRP Ann. Manuf. Technol.* **2021**, *70*, 261–264. [[CrossRef](#)]
14. Braunovic, M. Effect of connection design on the contact resistance of high power overlapping bolted joints. *IEEE Trans. Compon. Packag. Technol.* **2002**, *25*, 642–650. [[CrossRef](#)]
15. Melsom, S.W.; Booth, H.C. The efficiency of overlapping joints in copper and aluminium busbar conductors. *J. Inst. Electr. Eng.* **1922**, *60*, 889–899. [[CrossRef](#)]
16. *ASTM E8/E8 M*; Standard Test Methods for Tension Testing of Metallic Materials. ASTM International: West Conshohocken, PA, USA, 2016.
17. *ISO 898-1:2013*; Mechanical Properties of Fasteners Made of Carbon Steel and Alloy Steel-Part 1: Bolts, Screws and Studs with Specified Property Classes-Coarse Thread and Fine Pitch Thread. ISO—International Organization for Standardization: Geneva, Switzerland, 2013.
18. *ISO 898-2:2012*; Mechanical Properties of Fasteners Made of Carbon Steel and Alloy Steel-Part 2: Nuts with Specified Property Classes-Coarse Thread and Fine Pitch Thread. ISO—International Organization for Standardization: Geneva, Switzerland, 2012.
19. *IEEE Std C37.20.2*; IEEE Standard for Metal-Clad Switchgear. IEEE Power and Energy Society: New York, NY, USA, 2015.
20. Kumar, N.; Masters, I.; Das, A. In-depth evaluation of laser-welded similar and dissimilar material tab-to-busbar electrical interconnects for electric vehicle battery pack. *J. Manuf. Processes* **2021**, *70*, 78–96. [[CrossRef](#)]
21. MatWeb. Available online: <https://www.matweb.com> (accessed on 1 May 2022).
22. Nielsen, C.V.; Martins, P.A.F. Finite element flow formulation. In *Metal Forming: Formability, Simulation and Tool Design*; Academic Press: London, UK, 2021; pp. 181–249.
23. Studer, F.J. Contact resistance in spot welding. *Weld. J.* **1939**, *18*, 374–380.
24. Reichel, A.; Sampaio, R.; Pragana, J.; Bragança, I.; Silva, C.; Martins, P. Form-fit joining of hybrid busbars using a flexible tool demonstrator. *Proc. Inst. Mech. Eng. Part L J. Mater. Des. Appl.* **2021**, *236*, 1164–1175. [[CrossRef](#)]